Role of Ni and Zn Dopants in Modulating the Structure and Photocatalytic Activity of Mesoporous Silica–Cu Catalysts for Methylene Blue Degradation

Maria Ulfa [1]*, Suwiji Lestari[1]

[1] Chemistry Education Study Program, Faculty of Teacher Training and Education, Universitas Sebelas Maret, Surakarta 57126, Indonesia

* Corresponding Author. E-mail: ulfa.maria2015@gmail.com; mariaulfa@staff.uns.ac.id

(M. Ulfa)

Telp: +62-81392932270

Abstract

This study investigates the structural and photocatalytic roles of Ni and Zn dopants in mesoporous silica–Cu catalysts for methylene blue degradation under light irradiation. The materials were synthesized and systematically characterized using FTIR, XRD, BET, SEM–EDS, and UV–DRS to elucidate dopant-dependent structural, textural, and electronic modifications. XRD analysis revealed that Zn doping enhances crystallinity to 90.80% with a crystallite size of 1.97 nm, whereas Ni doping produces lower crystallinity (80.69%) and smaller crystallites (1.82 nm), indicating defect-rich microstructures. BET analysis confirmed mesoporous characteristics in both systems, with Zn incorporation generating broader pore distributions and higher adsorption capacity, while Ni induces more confined pore structures. SEM results showed average particle sizes of 1.49 nm for Zn-doped and 1.67 nm for Ni-doped catalysts. UV–DRS measurements demonstrated pronounced electronic modulation, with Ni doping significantly narrowing the band gap to 1.02–1.11 eV compared with 2.08–2.78 eV for Zn-doped materials. Photocatalytic evaluation at an initial methylene blue concentration of 5 ppm showed superior performance for the Ni-doped catalyst, achieving 79.59% removal efficiency and an adsorption capacity of 19.89 mg g^{-1}, compared with 50.98% removal and 12.74 mg g^{-1} for the Zn-doped system. Kinetic analysis followed pseudo-first-order behavior, with a higher rate constant for Ni doping (0.01675 min^{-1}) than Zn doping (0.00706 min^{-1}). These findings demonstrate that Ni primarily enhances photocatalytic activity through electronic defect formation and band gap narrowing, while Zn mainly improves structural ordering and pore accessibility. The study highlights the critical role of dopant selection in tailoring

structure–activity relationships in mesoporous silica–Cu photocatalysts.

Keywords: Mesoporous silica–Cu; Ni/Zn doping; Photocatalysis; Methylene blue; Band gap tuning; Structure–activity

Graphical Abstract

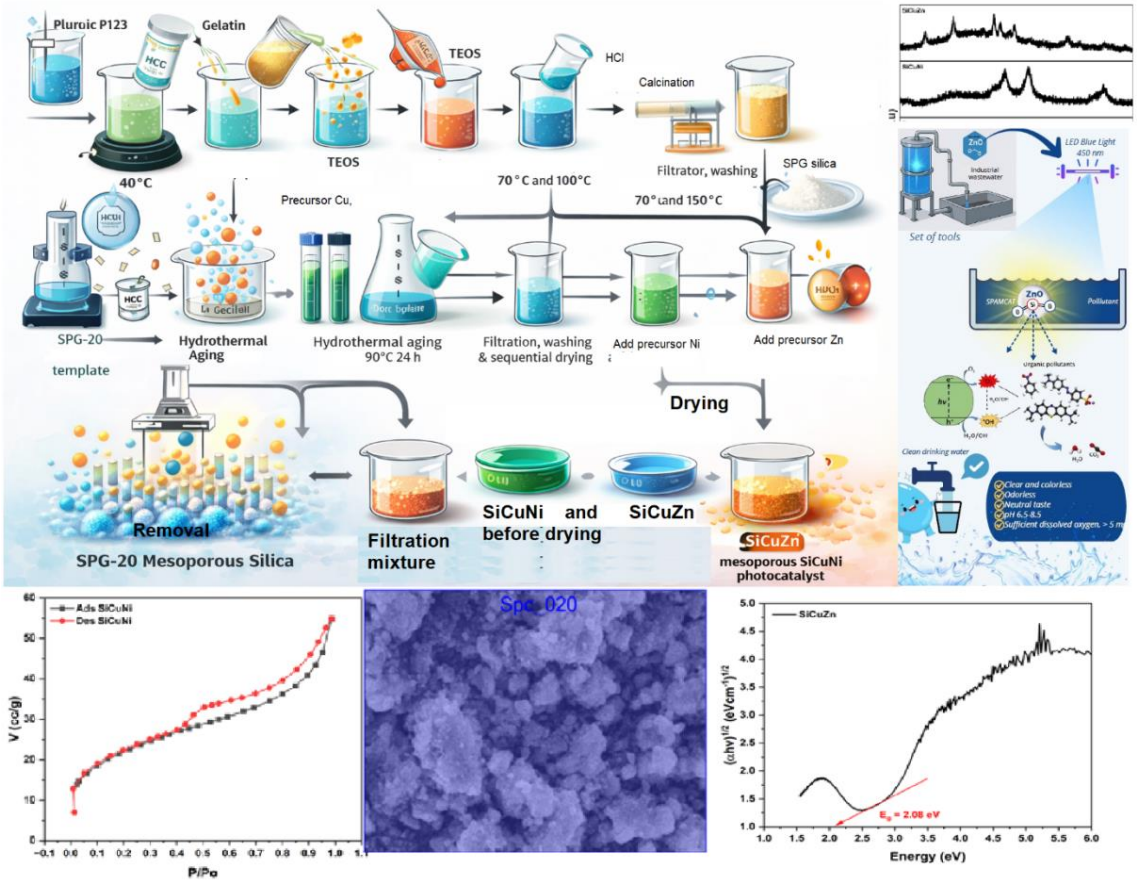

Introduction

The increasing discharge of synthetic dyes into aquatic environments has become a major global environmental concern, particularly due to their persistence, toxicity, and resistance to conventional treatment methods [1, 2]. Among these pollutants, methylene blue is widely used in textile, printing, and biomedical industries and is frequently detected in industrial wastewater [3-5]. Its stable aromatic structure and resistance to biodegradation make effective removal challenging, thereby necessitating the development of advanced treatment technologies [6-9].

Photocatalysis has emerged as a promising and sustainable approach for dye degradation because it enables the mineralization of organic contaminants into harmless end products using light energy, without generating secondary pollutants [9-10]. Mesoporous silica–based materials have attracted considerable attention as photocatalyst supports due to their high surface area, tunable pore structure, chemical stability, and excellent adsorption capacity [12-15]. When combined with transition metals such as copper, these materials exhibit enhanced catalytic properties resulting from improved charge separation and increased active sites [16, 17]. However, the photocatalytic performance of mesoporous silica–Cu systems is still limited by rapid electron–hole recombination and suboptimal light absorption efficiency [18, 19]. To overcome these limitations, the incorporation of secondary metal dopants has been widely explored as an effective strategy to modify structural, electronic, and surface properties [20, 21].

Transition metal dopants such as nickel (Ni) and zinc (Zn) are particularly attractive because of their distinct physicochemical characteristics and catalytic functionalities [22, 23]. Ni is known for its ability to introduce defect states and narrow band gap energy, thereby improving visible-light absorption and promoting charge carrier mobility [24-26]. These electronic modifications can enhance the generation of reactive oxygen species, which are essential for photocatalytic degradation [27, 28]. In contrast, Zn is often associated with improved crystallinity, structural stability, and enhanced adsorption behavior due to its ability to regulate particle growth and pore organization [29-31]. As a result, Ni and Zn dopants may influence photocatalytic performance through fundamentally different mechanisms, involving both electronic and structural modulation [32, 33]. Understanding how these dopants interact with mesoporous silica–Cu frameworks is therefore crucial for optimizing catalyst design. The incorporation of dopant species can alter crystallite size, pore distribution, surface morphology, and optical properties, all of which directly affect photocatalytic efficiency [34-36]. Furthermore, dopant-induced defect formation, band structure modification, and improved interfacial charge transfer can significantly enhance reaction kinetics during dye degradation [37, 38]. Despite growing interest in dopant engineering,

comparative studies examining the distinct roles of Ni and Zn within the same mesoporous silica–Cu system remain limited.

This study aims to systematically investigate the role of Ni and Zn dopants in modulating the structural characteristics and photocatalytic activity of mesoporous silica–Cu catalysts for methylene blue degradation. By correlating physicochemical properties with photocatalytic performance, this work seeks to clarify the mechanisms through which different dopants influence adsorption behavior, light absorption, and charge carrier dynamics. The findings are expected to provide deeper insight into dopant-dependent structure–activity relationships and offer design guidelines for developing highly efficient mesoporous photocatalysts for wastewater treatment applications.

Experimental Section

Materials

Materials used for the synthesis of the mesoporous SiCuNi photocatalyst comprised silica precursors, metal dopant sources, structure-directing agents, and auxiliary reagents for synthesis and photocatalytic evaluation. Tetraethyl orthosilicate (TEOS, Mr 208.33 g mol^{-1}, Sigma-Aldrich Merck KGaA) was employed as the primary silica source for framework formation. Commercial gelatin (average molecular weight ≈ 90,000 g mol^{-1}, Gelita) functioned as an organic template and structure-directing agent to promote mesoporous organization [39]. Mesoporous silica SPG-20 served as a hard template to regulate pore architecture and structural ordering. The active metal components consisted of copper and nickel precursors introduced to form the bimetallic catalytic system. Copper(II) nitrate trihydrate ($Cu(NO_3)_2 \cdot 3H_2O$, Sigma-Aldrich Merck KGaA) was used as the copper source, while nickel(II) nitrate hexahydrate ($Ni(NO_3)_2 \cdot 6H_2O$, Sigma-Aldrich Merck KGaA) served as the nickel precursor. These metal salts were selected due to their high solubility and ability to generate well-dispersed metal oxide species within the silica framework after thermal treatment. Hydrochloric acid (37% HCl, Mr 36.5 g mol^{-1}, Sigma-Aldrich Merck KGaA) was used to catalyze hydrolysis and condensation reactions during silica network formation and to regulate solution acidity. Sodium hydroxide solution (1–2 M NaOH, Mr 39.997 g mol^{-1}, Sigma-Aldrich Merck

KGaA) was applied for alkaline extraction of the hard silica template following thermal processing. Deionized water was used as the solvent throughout all synthesis stages.For photocatalytic performance evaluation, methylene blue (Mr 319.85 g mol^{-1}, Sigma-Aldrich Merck KGaA) was used as the model organic pollutant. Photocatalytic experiments were conducted using a visible-light photoreactor equipped with a mechanical shaker, and concentration changes were monitored using UV–Vis spectrophotometry at a wavelength of 665 nm.

Synthesis of SiCuNi Mesoporous Photocatalyst

Gelatin-modified SPG-20 mesoporous silica was first prepared and subsequently used as the hard template for SiCuNi synthesis. Pluronic P123 (4 g) and gelatin (0.8 g) were dissolved and homogenized at 40°C under continuous stirring. A hydrochloric acid solution (prepared by diluting 19.5 mL of 37% HCl in 127 mL deionized water) was added dropwise to promote micelle formation and regulate the acidic environment. Tetraethyl orthosilicate (TEOS) was then introduced gradually, and the mixture was stirred for 24 h to allow hydrolysis and condensation. The resulting gel underwent hydrothermal aging at 90 °C for 24 h, followed by filtration, washing, sequential drying at 70 °C and 100 °C, and final calcination at 550 °C for 5 h to remove organic templates and obtain gelatin-modified SPG-20 mesoporous silica. For SiCuNi synthesis, 1.25 g of the prepared SPG-20 was used as the hard template. Copper and nickel precursors were dissolved separately in deionized water and combined under magnetic stirring for 1 h to form a homogeneous Cu–Ni bimetallic solution. Gelatin was dissolved in deionized water to produce a viscous solution, into which the Cu–Ni solution was incorporated with continuous stirring. TEOS was then added dropwise as the silica precursor, followed by gradual addition of an acid catalyst to accelerate hydrolysis and condensation. The mixture was maintained at approximately 70 °C for 1 h to promote network formation and partial solvent removal, then dried at 100 °C for 24 h to obtain a solid precursor.

The dried material was thermally treated at 250 °C for 5 h to stabilize the inorganic framework and partially remove organics. The hard template was subsequently removed by alkaline extraction in 100 mL of 1 M NaOH at 90 °C for 10 h. The product was washed repeatedly with deionized water until neutral pH and dried overnight at 60 °C, yielding the mesoporous

SiCuNi photocatalyst. The SiCuZn catalyst was synthesized following the same preparation procedure, with the only difference being the substitution of the nickel precursor with an appropriate zinc precursor during the bimetallic solution preparation stage.

Photodegradation of Methylene Blue

The photocatalytic performance of the synthesized materials was evaluated through the degradation of methylene blue under visible-light irradiation. A 200 mL aqueous solution of methylene blue with an initial concentration of 5 ppm was transferred into a photocatalytic reactor, followed by the addition of 50 mg of the SiCuNi photocatalyst. The suspension was magnetically stirred in the dark for 30 minutes to establish adsorption–desorption equilibrium between the dye molecules and the catalyst surface. After equilibration, the reaction mixture was distributed into twelve dark glass vials, each containing 10 mL of suspension. One vial was designated as the initial concentration reference (C_0), while the remaining vials were placed in the photocatalytic reactor equipped with a mechanical shaker and a visible-light source. During irradiation, aliquots were collected at regular intervals, every 5 minutes up to 20 minutes, followed by sampling every 10 minutes until 90 minutes of reaction time. Each collected sample was immediately sealed and stored in dark conditions to prevent further photoreaction. The residual concentration of methylene blue was determined by measuring the absorbance of each sample using a UV–Vis spectrophotometer at a wavelength of 665 nm, allowing quantitative monitoring of dye degradation throughout the photocatalytic process.

Result and Discussion

FTIR

The FTIR spectra of the mesoporous silica–Cu catalysts doped with Ni and Zn reveal distinct structural modifications induced by the dopants. The broad absorption band around 3400 cm^{-1} corresponds to the stretching vibrations of surface –OH groups and adsorbed water molecules, indicative of hydroxylated silica surfaces [40, 41]. Notably, the intensity of this band decreases upon Ni doping, suggesting partial condensation of silanol groups and a potential alteration of surface hydrophilicity.

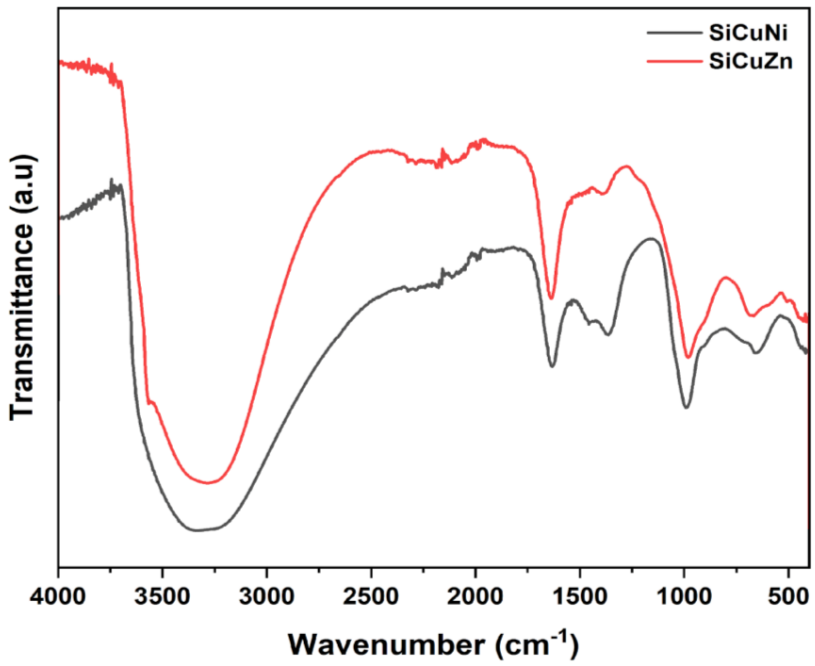

Figure 1. FTIR spectra of SiCuNi and SiCuZn mesoporous silica–Cu photocatalysts

The prominent bands in the region of 1000–1200 cm^{-1} are characteristic of Si–O–Si asymmetric stretching vibrations, reflecting the mesoporous silica framework [42, 43]. The Zn-doped mesoporous silica–Cu catalyst exhibits a higher transmittance in this region compared to the Ni-doped mesoporous silica–Cu catalyst, implying that Zn incorporation preserves the silica network more effectively, whereas Ni dopants introduce subtle distortions or defects within the silica matrix [44]. Additionally, the lower wavenumber bands (~450–800 cm^{-1}) correspond to M–O (M = Cu, Ni, Zn) vibrations, signifying successful incorporation of metal dopants into the silica framework or formation of metal oxide clusters [45]. The differences in these bands between the Ni- and Zn-doped catalysts indicate that the two dopants influence the local coordination environment and bonding interactions differently. Collectively, these structural modulations, as revealed by FTIR, correlate with the observed photocatalytic performance in Methylene Blue degradation. Ni doping likely enhances electron–hole separation due to defect-induced electronic states, while Zn doping maintains framework integrity and optimizes active site accessibility [46, 47]. Hence, the choice of dopant critically governs both the physicochemical structure and

photocatalytic efficiency of mesoporous silica–Cu catalysts. The FTIR spectrum of the SiCuZn sample exhibits an absorption band above 3500 cm^{-1}, indicating the presence of specific hydroxyl species on the surface. The shoulder observed above 3500 cm^{-1} in the FTIR spectrum of SiCuZn can be attributed to the stretching vibrations of hydroxyl (–OH) groups, particularly those that are isolated or weakly hydrogen-bonded. In contrast to the broad band typically found around 3200–3400 cm^{-1}, which is associated with strongly hydrogen-bonded –OH groups (such as adsorbed water or interacting silanol groups), the presence of a shoulder at higher wavenumbers indicates the existence of free silanol (Si–OH) groups on the silica surface. This feature suggests a heterogeneous hydroxyl environment, likely influenced by Zn incorporation, which modifies the surface structure and reduces the extent of hydrogen bonding among hydroxyl groups [64]. In the mid-infrared region, several characteristic absorption bands provide insight into the presence of surface functional groups and adsorbed species. The band around 1630 cm^{-1} is associated with the H–O–H bending vibration of adsorbed water, while the bands at 1400–1500 cm^{-1} originate from the vibrations of –OH (silanol) groups or residual organic groups from the synthesis process.

XRD

The XRD patterns of the mesoporous silica–Cu catalysts doped with Ni and Zn exhibit distinct differences in crystallographic features, confirming the structural influence of each dopant. Both samples display diffraction features associated with the amorphous–mesoporous silica matrix, typically observed as broad reflections at low diffraction angles, indicating that the mesoporous framework is retained after metal incorporation. However, differences in peak sharpness and intensity clearly distinguish the two doped systems. The Zn-doped mesoporous silica–Cu catalyst exhibits sharper and more intense diffraction lines compared to the Ni-doped counterpart, indicating a higher degree of structural ordering and crystallinity. This observation is quantitatively supported by the crystallinity values, where the Zn-doped sample reaches 90.80%, significantly higher than the Ni-doped sample at 80.69%. The enhanced crystallinity suggests that Zn incorporation promotes more ordered crystal growth or stabilizes crystalline domains within the silica–Cu matrix.In contrast, the Ni-doped catalyst shows relatively broader peaks and slightly

reduced intensity, reflecting smaller coherent crystalline domains and increased structural disorder. This is consistent with the calculated crystallite size, where the Ni-doped sample exhibits a smaller crystallite size (1.82 nm) compared to the Zn-doped sample (1.97 nm). The reduced crystallite size and lower crystallinity indicate that Ni incorporation induces lattice distortion or defect formation, which may originate from differences in ionic radius, coordination preference, or interaction strength with the silica framework.The reference diffraction lines confirm the presence of Cu, Ni, Zn, and SiO_2 phases, suggesting successful incorporation of the metal components within the mesoporous silica matrix without complete phase segregation. The relative peak distribution further indicates that Zn promotes more stable crystalline arrangements, whereas Ni contributes to defect-rich microstructures.These structural differences are highly relevant to photocatalytic behavior. The higher crystallinity and slightly larger crystallite size in the Zn-doped catalyst suggest improved structural stability and preserved framework integrity, which may enhance active site accessibility and facilitate charge transport along ordered domains [23, 48]. Conversely, the smaller crystallite size and increased structural defects introduced by Ni doping may generate localized electronic states that improve electron–hole separation, potentially enhancing photocatalytic reactivity despite the lower crystallinity [26, 49]. Overall, the XRD analysis demonstrates that Zn acts primarily as a crystallinity-enhancing dopant that stabilizes the mesoporous silica–Cu framework, while Ni functions as a defect-inducing dopant that modifies the microstructure and electronic properties [44, 50]. These contrasting structural roles directly support the dopant-dependent modulation of photocatalytic performance in Methylene Blue degradation.

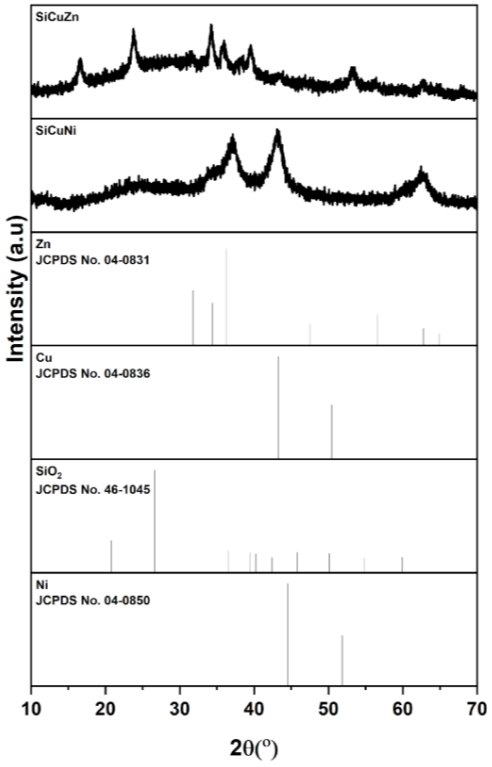

Figure 2. XRD patterns of SiCuNi and SiCuZn mesoporous silica–Cu photocatalysts with corresponding standard diffraction references (JCPDS) of Zn, Cu, SiO_2, and Ni.

Table 1. Crystallite Size and Degree of Crystallinity of Mesoporous SiCuNi and SiCuZn Photocatalysts

Sample	D (nm)	Crystallinity (%)
SiCuNi	1.82	80.69
SiCuZn	1.97	90.80

The nitrogen adsorption–desorption isotherms of the Ni- and Zn-doped mesoporous silica–Cu catalysts exhibit typical type IV isotherm characteristics with a clear hysteresis loop, confirming the presence of mesoporous structures [51]. This behavior indicates that both materials retain well-developed mesoporosity after metal incorporation, which is essential for effective mass transport and catalytic accessibility [52]. Notably, significant differences are observed in the adsorption capacity and pore structure between the two doped systems. The Zn-doped mesoporous silica–Cu catalyst shows substantially higher nitrogen uptake across the entire relative pressure range,

particularly at high P/P₀ values. This suggests a larger total pore volume and a more developed mesoporous network compared to the Ni-doped catalyst. The sharper increase in adsorption at higher relative pressure also indicates enhanced capillary condensation, reflecting the presence of wider or more accessible mesopores [53, 54].

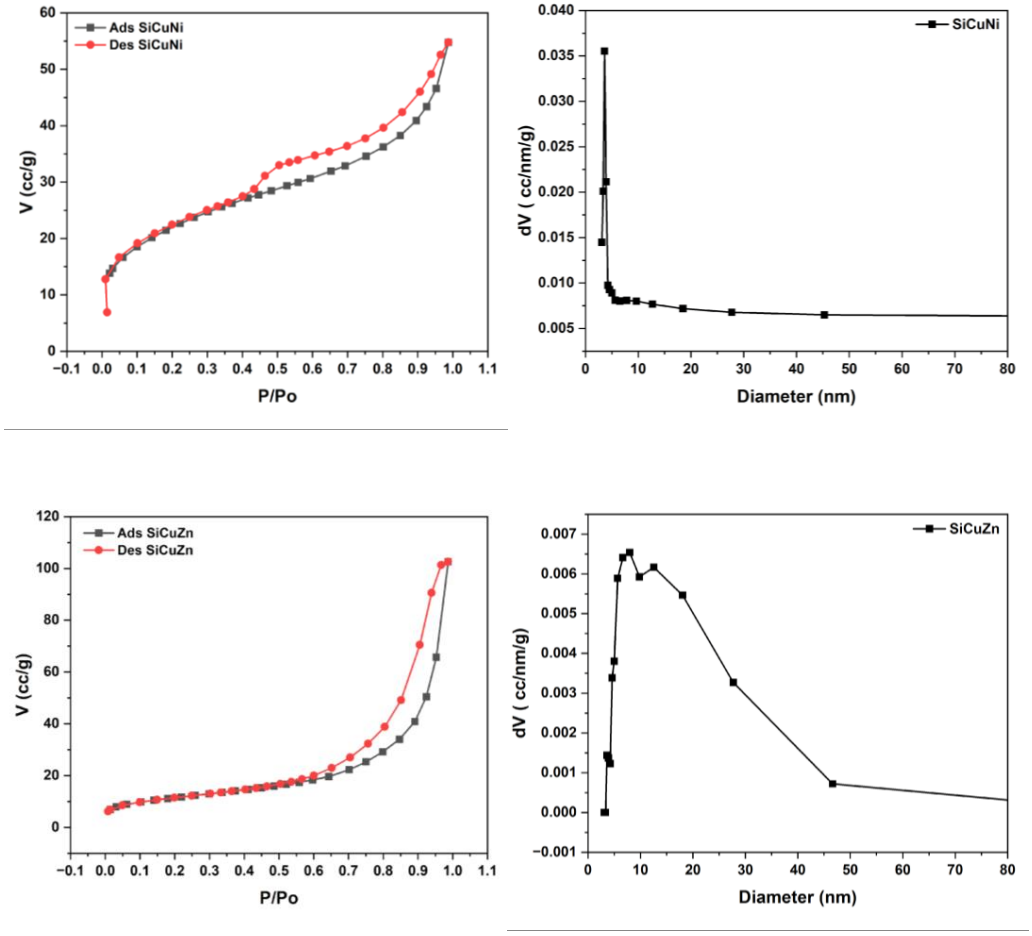

Figure 3. Nitrogen Adsorption–Desorption Isotherms and Pore Size Distribution of Mesoporous SiCuNi and SiCuZn Photocatalysts

By comparison, the Ni-doped catalyst exhibits lower adsorption capacity and a more gradual adsorption profile, suggesting a relatively reduced pore volume and possible partial pore blocking or structural contraction. This behavior implies that Ni incorporation may introduce framework distortion or promote partial collapse or narrowing of pore channels, consistent with its defect-inducing structural role observed in crystallographic analysis. The pore size distribution further

supports these observations. The Ni-doped sample displays a narrow distribution dominated by smaller mesopores, indicating more confined pore structures and lower pore accessibility. In contrast to this behavior, the Zn-doped catalyst shows a broader pore size distribution extending toward larger mesopore diameters, suggesting a more open and interconnected pore network. The presence of wider mesopores in the Zn-containing material enhances molecular diffusion and improves accessibility to active sites. These textural differences have direct implications for photocatalytic performance. The higher pore volume and broader mesopore distribution of the Zn-doped catalyst favor improved mass transfer, enhanced adsorption of methylene blue molecules, and greater exposure of catalytic active sites [55]. At the same time, the smaller and more confined pores in the Ni-doped system may limit diffusion but can enhance surface interactions and charge separation through defect-rich structures [56]. Taken together, the adsorption–desorption analysis demonstrates that Zn doping primarily enhances textural development by preserving and expanding the mesoporous framework, whereas Ni doping tends to compact or distort the pore structure. This complementary structural modulation highlights the dopant-dependent control of surface area, pore architecture, and catalytic accessibility in mesoporous silica–Cu systems.

The morphological characteristics of the Ni- and Zn-doped mesoporous silica–Cu catalysts reveal aggregated granular structures with irregular particle shapes, indicating the formation of clustered nanostructured domains [57]. Both samples exhibit relatively uniform particle assemblies, suggesting that metal incorporation does not disrupt the overall particle formation mechanism but influences particle growth and packing behavior. Quantitative particle size analysis shows slight differences between the two doped systems. The Ni-doped mesoporous silica–Cu catalyst exhibits an average particle diameter of 1.67 nm, while the Zn-doped sample shows a slightly smaller average particle diameter of 1.49 nm. The histogram distributions indicate relatively narrow particle size distributions for both materials, reflecting controlled nucleation and growth during synthesis. The smaller particle size observed in the Zn-doped catalyst suggests that Zn incorporation may inhibit particle coalescence or limit crystal growth, leading to more finely dispersed domains. In contrast, the slightly larger particle size in the Ni-doped sample may be

associated with stronger metal–framework interactions or localized structural distortion that promotes particle aggregation. This behavior is consistent with previous structural analyses indicating that Ni tends to induce defect formation and microstructural distortion within the silica–Cu matrix [58]. Elemental composition analysis further confirms successful incorporation of metal dopants into the mesoporous silica framework. The Ni-doped catalyst shows significant Ni content alongside Cu, O, C, and Si, indicating effective metal loading and integration within the host matrix. The Zn-doped catalyst similarly demonstrates the presence of Zn and Cu with comparable oxygen and silica content, confirming the formation of a multicomponent metal–silica system.

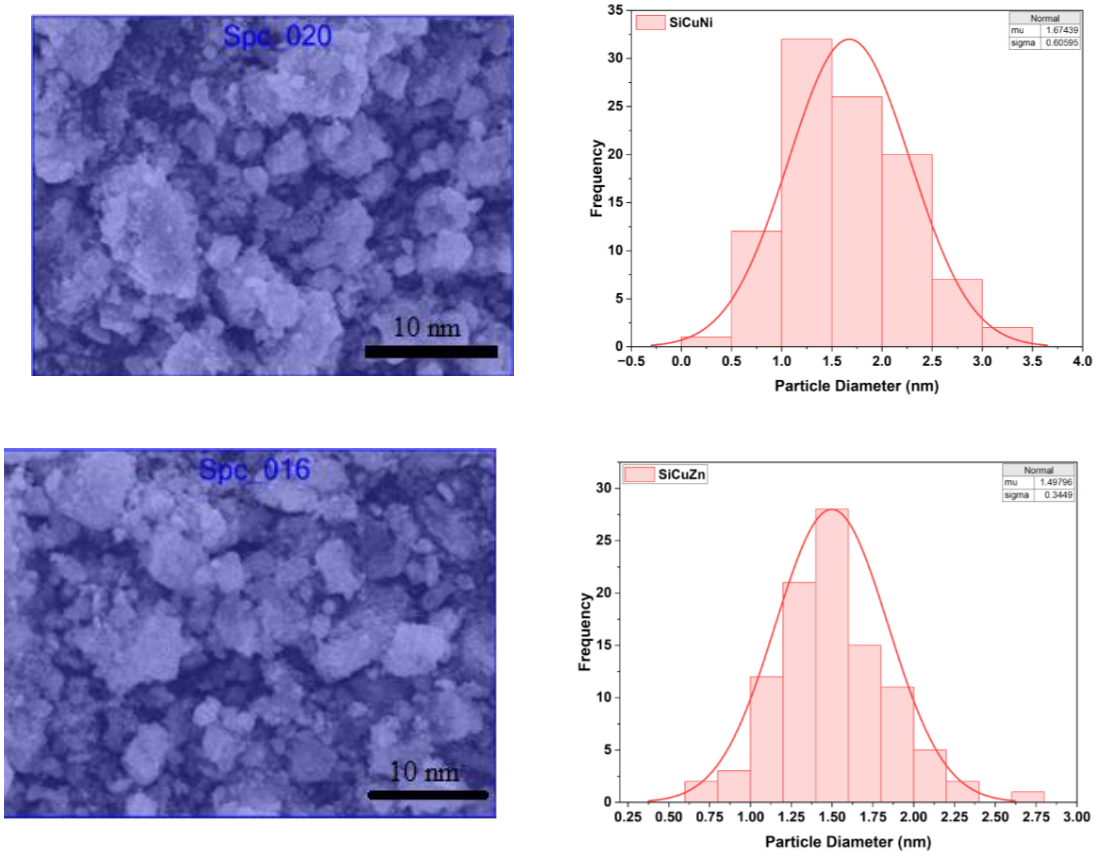

Figure 4. Morphological Characteristics and Particle Size Distribution of Mesoporous SiCuNi and SiCuZn Photocatalysts

Tablel 2. Synthesis Ratio, Particle Size, and Post-Characterization Elemental Distribution of SiCuNi and SiCuZn

Sample	Elemental Ratio During Synthesis	Diameter (nm)	Elemental Composition Analysis (%)						Elemental Ratio After Characterization
			Ni	Cu	Zn	C	O	Si	
SiCuNi	Ni : Cu = 2 : 1	1.67	41.15	11.35	–	5.69	33.60	8.20	Ni : Cu = 3.625 : 1
SiCuZn	Cu : Zn = 1 : 1	1.49	–	24.62	19.68	5.99	33.31	10.67	Cu : Zn = 1.25 : 1

Comparison between the synthesis ratio and post-characterization elemental ratio reveals changes in relative metal distribution, suggesting that metal incorporation efficiency and dispersion differ between the two dopants. The Ni-containing sample exhibits a higher relative Ni-to-Cu ratio after characterization, indicating preferential stabilization or stronger retention of Ni within the structure. Meanwhile, the Zn-containing catalyst shows a more balanced Cu–Zn distribution, which may reflect more homogeneous metal dispersion within the mesoporous framework.

These morphological and compositional differences have important implications for catalytic behavior. The smaller particle size and more uniform dispersion in the Zn-doped system may enhance surface accessibility and active site exposure, supporting efficient adsorption and diffusion processes [46]. Conversely, the slightly larger particle size and higher defect density in the Ni-doped catalyst may promote localized electronic interactions that improve charge separation efficiency [59]. Taken together, the morphological, particle size, and compositional analyses confirm that both dopants are successfully incorporated into the mesoporous silica–Cu structure but influence particle growth, dispersion, and elemental distribution in distinct ways. Zn doping favors finer particle dispersion and more homogeneous metal distribution, whereas Ni doping promotes defect-rich structures with slightly larger aggregated domains. These differences further support the dopant-dependent modulation of structural and catalytic properties in mesoporous silica–Cu systems.

The optical properties of the Ni- and Zn-doped mesoporous silica–Cu catalysts were investigated using UV–Vis diffuse reflectance spectroscopy (UV–DRS), and the band gap energies were estimated using Tauc plot analysis. The absorption behavior of both materials indicates strong light interaction across the visible region, confirming that metal incorporation significantly modifies the electronic structure of the silica–Cu framework.The Ni-doped mesoporous silica–Cu catalyst exhibits relatively low band gap energies, estimated at approximately 1.11 eV and 1.02 eV from the corresponding Tauc plots. These narrow band gap values indicate the presence of defect-induced electronic states or intermediate energy levels within the band structure [60]. The incorporation of Ni likely introduces localized electronic states that facilitate electron excitation at lower photon energies, thereby enhancing visible-light absorption capability [61]. This band gap narrowing is consistent with the structural distortion and defect formation previously observed in crystallographic and textural analyses [62]. In comparison, the Zn-doped mesoporous silica–Cu catalyst shows significantly higher band gap energies, estimated at approximately 2.78 eV and 2.08 eV. These values suggest that Zn incorporation preserves a more ordered electronic structure with fewer defect-related states compared to Ni doping. The wider band gap indicates that the Zn-containing material requires higher photon energy for electronic excitation, reflecting reduced electronic disorder and stronger structural integrity of the mesoporous framework. Despite the wider band gap, Zn doping still enhances optical absorption relative to undoped systems by modifying the electronic environment of Cu and silica. The presence of Zn may influence metal–oxygen bonding and electronic coupling within the framework, leading to improved charge mobility while maintaining structural stability. The distinct band gap differences between the two doped systems have important implications for photocatalytic performance. The narrower band gap of the Ni-doped catalyst promotes efficient visible-light harvesting and facilitates electron excitation, which can enhance charge carrier generation. Meanwhile, the wider band gap of the Zn-doped catalyst may suppress excessive recombination by maintaining a more stable electronic structure and better charge transport pathways. Overall, UV–DRS analysis demonstrates that Ni and Zn dopants modulate the electronic structure of mesoporous silica–Cu catalysts in fundamentally different ways. Ni doping strongly reduces band gap energy through defect-induced states and

enhanced visible-light absorption, whereas Zn doping maintains a wider band gap associated with structural stability and controlled electronic transitions. These contrasting electronic modifications contribute to the dopant-dependent photocatalytic behavior observed in methylene blue degradation.

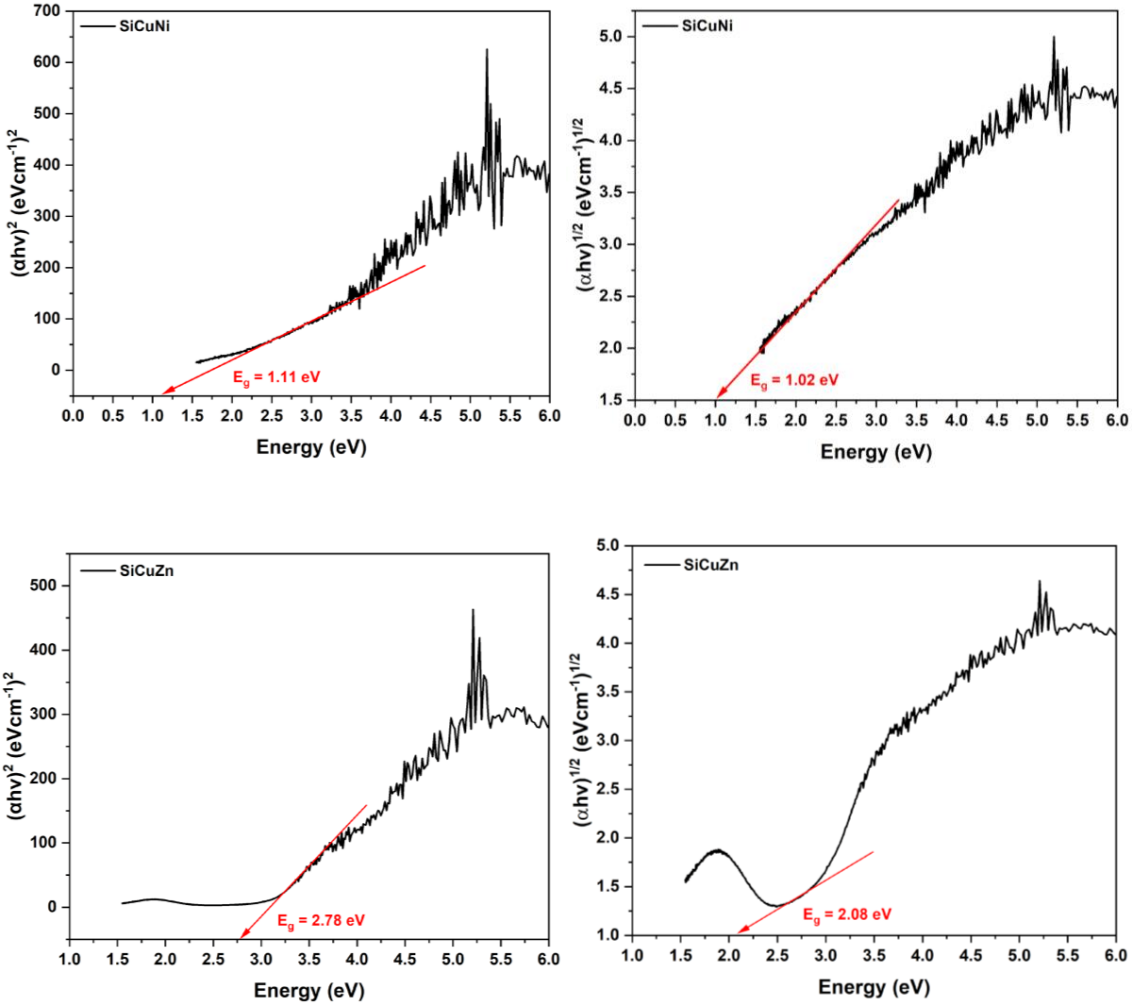

Figure 5. UV–Vis DRS Profiles and Direct–Indirect Optical Band Gap Analysis of SiCuNi and SiCuZn

The comparative results clearly show that both Ni- and Zn-doped mesoporous silica–Cu catalysts exhibit photocatalytic activity toward methylene blue degradation, yet their performance differs substantially. At an initial concentration of 5 ppm, the Ni-doped catalyst achieves a removal efficiency of 79.59% with an experimental adsorption capacity of 19.89 mg g^{-1}, whereas the Zn-

doped material shows a lower removal efficiency of 50.98% and qe of 12.74 mg g^{-1}. These differences indicate that Ni incorporation significantly improves the overall degradation performance. Kinetic evaluation further supports this trend. The pseudo-first-order model provides a good description of the reaction behavior for both catalysts, with comparable correlation coefficients ($R^2 \approx 0.867$ for SiCuNi and 0.859 for SiCuZn). However, the reaction rate constant for the Ni-doped system (k_1 = 0.01675 min^{-1}) is more than twice that of the Zn-doped catalyst (k_1 = 0.00706 min^{-1}), indicating substantially faster degradation kinetics. This suggests that Ni incorporation enhances reactive species generation and improves the interaction between the catalyst surface and methylene blue molecules.

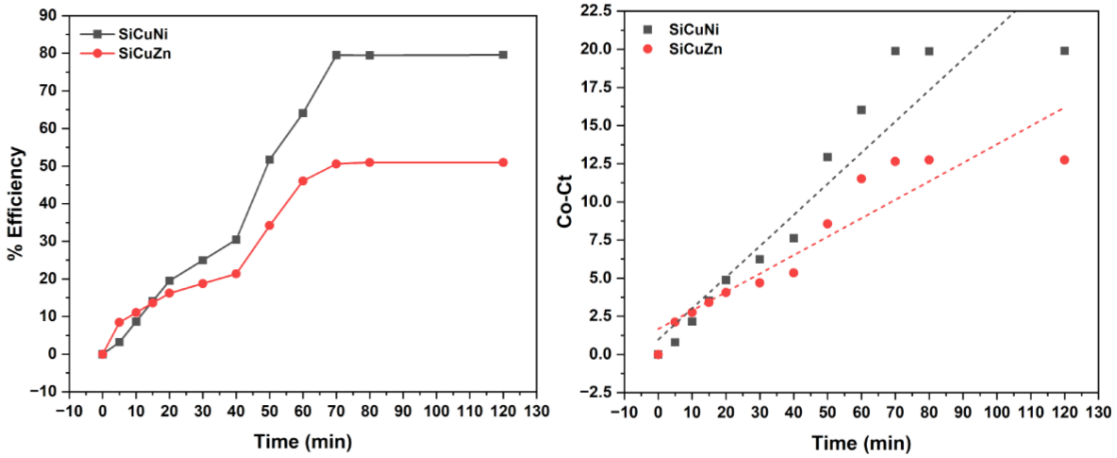

a. **b.**

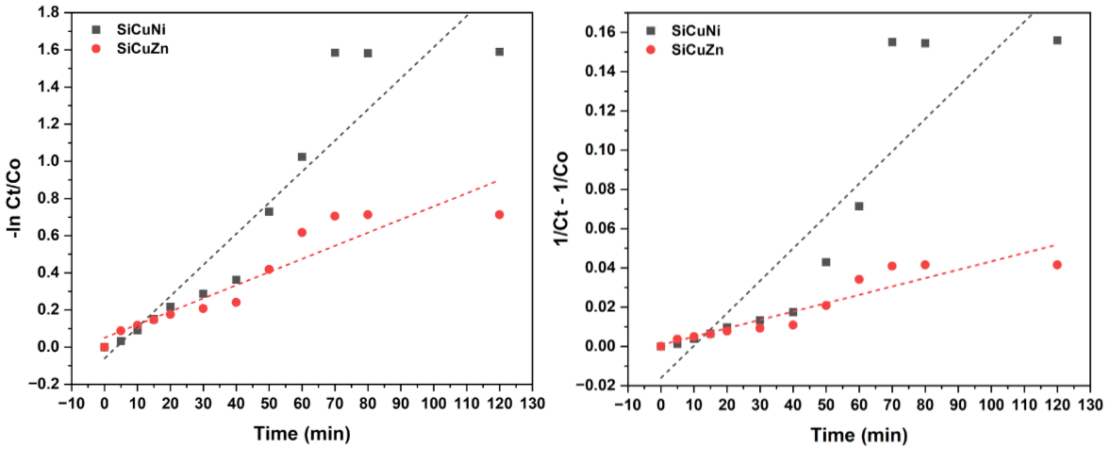

c. **d.**

Figure 6. Photodegradation of Methylene Blue (a). and Kinetic Analysis Based on Pseudo-Zero- (b), First- (c), and Second (d)-Order Models over SiCuNi and SiCuZn

Tabel 3. Rate Constants and Model Fitting Results for Pseudo-Zero, First, and Second-Order Kinetics

Sample	C_o (ppm)	q_e Exp (mg/g)	Removal Efficiency, %	Pseudo Zero Order			Pseudo First Order			Pseudo Second Order		
				q_e Cal (mg/g)	K_1 (min^{-1})	R^2	q_e Cal (mg/g)	K_1 (min^{-1})	R^2	q_e Cal (mg/g)	K_2 ($g.mg^{-1}.min^{-1}$)	R^2
SiCuNi	10	19.89	79.59	0.97933	0.2041	0.87456	-0.06026	0.01675	0.8674	-0.0161	0.00165	0.81535
SiCuZn	10	12.74	50.98	1.6713	0.121	0.85333	0.05088	0.00706	0.85888	7.35852E-4	4.26061E-4	0.85483

The adsorption–reaction characteristics are also consistent with the higher activity of the Ni-doped material. Its higher experimental adsorption capacity indicates more effective pollutant capture prior to photodegradation, which can facilitate subsequent oxidative reactions. In contrast, the lower qe value of the Zn-doped catalyst suggests weaker adsorption interaction, which may limit degradation efficiency despite its structurally stable framework.Model comparison shows that the pseudo-zero-order model produces relatively high R^2 values for both materials (0.875 for SiCuNi and 0.853 for SiCuZn), but the pseudo-first-order model better reflects the photocatalytic mechanism involving surface-mediated reactions and concentration-dependent kinetics. The pseudo-second-order model yields lower correlation values, indicating that chemisorption is not the dominant rate-controlling step under the studied conditions. From a structure–activity perspective, the superior performance of the Ni-doped catalyst can be associated with enhanced electronic properties that promote charge carrier generation and separation, leading to faster reaction kinetics. Meanwhile, Zn incorporation appears to provide moderate photocatalytic activity, possibly linked to improved structural organization or pore characteristics, but without sufficiently enhancing electronic activation for efficient photodegradation. Overall, the experimental data consistently demonstrate that Ni incorporation produces stronger improvements in photocatalytic efficiency, reaction kinetics, and adsorption capacity compared to Zn doping. These findings

highlight the dominant role of electronic modification in governing photocatalytic degradation performance, while structural or textural improvements alone are insufficient to achieve comparable activity under the same operating conditions.

Under light irradiation, the photocatalytic process begins with photon absorption by the doped mesoporous silica–Cu system, leading to the excitation of electrons from the valence band to the conduction band and the formation of electron–hole pairs. In the Ni-doped catalyst, the presence of Ni-related electronic states facilitates more efficient charge separation by acting as trapping centers that suppress rapid electron–hole recombination. The photogenerated electrons are transferred to surface-adsorbed oxygen molecules, producing superoxide radicals ($\bullet O_2^-$), while the photogenerated holes react with surface hydroxyl groups or water molecules to form hydroxyl radicals ($\bullet OH$). These highly reactive oxygen species are primarily responsible for oxidative degradation of methylene blue molecules adsorbed on the catalyst surface, proceeding through progressive breakdown into smaller intermediate organic species, with potential further mineralization toward CO_2 and H_2O. In contrast, the Zn-doped system follows the same fundamental photocatalytic pathway but with lower efficiency in charge carrier utilization. The wider effective band gap and weaker electron trapping capability reduce visible-light absorption and increase the likelihood of electron–hole recombination before reactive species can form [63]. Although Zn incorporation may enhance pore accessibility and improve diffusion of reactants to active sites, the generation rate of reactive oxygen species remains comparatively limited.

In addition to structural and optical properties, the oxidation state of copper significantly influences the photocatalytic mechanism. The valence state of Cu in the catalyst is predominantly present as Cu^{2+} and/or Cu^{+} species, which play a crucial role in the photocatalytic mechanism. Cu^{2+} acts as an electron trapping center by capturing photogenerated electrons to form Cu^{+}, thereby suppressing rapid electron–hole recombination. Subsequently, Cu^{+} can transfer the trapped electrons to adsorbed oxygen molecules, regenerating Cu^{2+} and producing reactive oxygen species such as superoxide radicals ($\bullet O_2^-$). This Cu^{2+}/Cu^{+} redox cycle effectively enhances charge separation and promotes the formation of reactive species responsible for pollutant degradation [65]. However, the formation and transformation of intermediate species were not directly analyzed in this study.

As a result, fewer oxidative radicals participate in dye decomposition, leading to comparatively slower reaction kinetics and reduced overall degradation efficiency.These differences indicate that photocatalytic performance is governed not only by surface accessibility but also, more critically, by the effectiveness of electronic modulation in promoting charge separation and reactive species formation.

Conclusions

This study demonstrates that Ni and Zn dopants modulate the structure and photocatalytic behavior of mesoporous silica–Cu catalysts through fundamentally different mechanisms. Zn incorporation primarily enhances structural ordering and textural development, as reflected by higher crystallinity (90.80%) and slightly larger crystallite size (1.97 nm) compared to the Ni-doped sample (80.69% and 1.82 nm). It also produces smaller and more uniformly dispersed particles (1.49 nm vs 1.67 nm), broader mesopore distribution, and higher pore accessibility. In contrast, Ni incorporation induces defect-rich microstructures, significantly narrows the band gap (≈1.02–1.11 eV compared to 2.08–2.78 eV for Zn doping), and promotes more efficient charge separation, indicating stronger electronic activation. These structural and electronic differences are directly reflected in photocatalytic performance. The Ni-doped catalyst achieves substantially higher methylene blue removal efficiency (79.59%) and adsorption capacity (19.89 mg g^{-1}) than the Zn-doped catalyst (50.98% and 12.74 mg g^{-1}), along with faster pseudo-first-order kinetics (k_1 = 0.01675 min^{-1} vs 0.00706 min^{-1}). These results indicate that electronic structure modulation plays a more dominant role than textural improvement in determining photocatalytic efficiency. Ni doping therefore provides stronger activity enhancement through defect-mediated charge separation, while Zn doping mainly contributes to structural stabilization and improved pore organization.

Acknowledgements

The author gratefully acknowledges Universitas Sebelas Maret (UNS) for the financial support received through the Research Excellence Grant Scheme (PUTA UNS) 2026. The provision of this funding greatly facilitated the accomplishment of the present study and enabled meaningful contributions to the advancement of scientific research under the auspices of this distinguished institution.

Conflict-of-Interest Statement

The authors declare that they have no known competing financial interests or personal relationships that could have appeared to influence the work reported in this paper

Author Contributions

Maria Ulfa: Conceptualization, Methodology, Resources, Supervision, Funding Acquisition, Writing – Review & Editing. Suwiji Lestari: Project Administration, Data Curation, Formal Analysis, Software. Maria Ulfa and Suwiji Lestari: Investigation, Writing – Original Draft, Validation, Visualization.

References

[1] Al-tohamy, R., Ali, S.S., Li, F., Okasha, K.M., Mahmoud, Y.A., Elsamahy, T., Jiao, H., Fu, Y., Sun, J. (2022). Ecotoxicology and Environmental Safety A critical review on the treatment of dye-containing wastewater : Ecotoxicological and health concerns of textile dyes and possible remediation approaches for environmental safety. *Ecotoxicology and Environmental Safety*, 231, 113160. DOI: 10.1016/j.ecoenv.2021.113160.

[2] Kumar, M., Pratap, V., Shahnaz, S., Bhat, B., Kumar, R. (2025). *Environmental risks of textile dyes and photocatalytic materials for sustainable treatment : current status and future directions*. Springer International Publishing.

[3] Olusakin, P., Oladiran, T., Oyinkansola, E., Joel, O. (2022). Results in Engineering Methylene blue dye : Toxicity and potential elimination technology from wastewater. *Results in Engineering*, 16(August), 100678. DOI: 10.1016/j.rineng.2022.100678.

[4] Modi, S., Yadav, V.K., Gacem, A., Ali, I.H., Dave, D., Khan, S.H., Yadav, K.K., Rather, S., Ahn, Y., Son, C.T. (2022). Recent and Emerging Trends in Remediation of Methylene Blue Dye from Wastewater by Using Zinc Oxide Nanoparticles

[5] Ulfa, M., Anggreani, C.N., Mulyani, B., Sholeha, N.A. (2024). Hexagonal TiO2/SiO2 Porous Microplates for Methylene Blue Photodegradation. *Bulletin of Chemical Reaction Engineering and Catalysis*, 19(1), 149–159. DOI: 10.9767/bcrec.20120.

[6] Oguilar, D.M.O., Norena, A.A.S., Tovar, M.A.M., Sanchez, J.V., Aparicio, J.R., Cacho, L.M., Betancourt, M.L.G. (2023). Adsorption and Photocatalytic Degradation of Methylene Blue in Carbon Nanotubes : A Review with Bibliometric Analysis

[7] Kabir, F., Ahovi, A., Albertinah, T. (2025). Current Research in Biotechnology Sustainable remediation of persistent organic Pollutants : A

review on Recent innovative technologies. *Current Research in Biotechnology*, 9(April), 100293. DOI: 10.1016/j.crbiot.2025.100293.

[8] González, S., Jaramillo-Fierro, X. (2025). Density Functional Theory Study of Methylene Blue Demethylation as a Key Step in Degradation Mediated by Reactive Oxygen Species. *International Journal of Molecular Sciences*, 26(4) DOI: 10.3390/ijms26041756.

[9] Bekele, T., Alamnie, G. (2025). Results in Chemistry The photocatalytic degradation of organic pollutants-a comprehensive overview. *Results in Chemistry*, 18(September), 102758. DOI: 10.1016/j.rechem.2025.102758.

[10] Khan, Y., Khan, M.N., Salam, A., Sadia, H., Ullah, M.F. (2024). Photocatalytic treatment of organic dyes using metal oxides and nanocomposites : A quantitative study. *Open Chemistry*, 22, 20240026. DOI: 10.1515/chem-2024-0026.

[11] Ulfa, M., Oktaviani, S.L., Mulyani, B., Sholeha, N.A. (2025). Metal Oxide for Fast Adsorption System in the Methylene Blue Removal. *Indonesian Journal of Chemistry*, 25(2), 619–637. DOI: 10.22146/ijc.92617.

[12] Zahoor, S., Muhammad, S., Kashif, M., Shahzad, N., Liu, Y., Celik, C., Ambreen, N., Ali, A., Wu, H., Azizi, S. (2026). Advances in mesoporous nanomaterials for photocatalytic degradation of pollutants : fundamentals , material classifications , challenges and future prospects. *Coordination Chemistry Reviews*, 549(P1), 217239. DOI: 10.1016/j.ccr.2025.217239.

[13] Wei, Y., Yang, W., Yang, Z. (2022). ScienceDirect An excellent universal catalyst support- mesoporous silica : Preparation , modification and applications in energy-related reactions. *International Journal of Hydrogen Energy*, 47(16), 9537–9565. DOI: 10.1016/j.ijhydene.2022.01.048.

[14] Kankala, R.K., Zhang, H., Liu, C., Kanubaddi, K.R., Lee, C., Wang, S., Cui, W., Santos, H.A., Lin, K., Chen, A. (2019). Metal Species – Encapsulated Mesoporous Silica Nanoparticles : Current Advancements and Latest Breakthroughs. 1902652, 1–42. DOI: 10.1002/adfm.201902652.

[15] Jovita, S., Tata, A., Santoso, E., Subagyo, R., Tamim, R., Asikin-mijan, N., Holilah, H., Bahruji, H., Edra, R. (2025). Mesoporous aluminosilicate from nanocellulose template : effect of porosity , morphology and catalytic activity for biofuel production. *Renewable Energy*, 250(May), 123293. DOI: 10.1016/j.renene.2025.123293.

[16] Hao, Y., Zhao, D., Liu, W., Zhang, M., Lou, Y., Wang, Z., Tang, Q., Yang, J. (2022). Uniformly Dispersed Cu Nanoparticles over Mesoporous Silica as a Highly Selective and Recyclable Ethanol Dehydrogenation Catalyst. *Catalyst*, 12, 1049. DOI: 10.3390/ catal12091049.

[17] Zhou, S., Yang, F., Wang, B., Su, H., Lu, K., Ding, Y., Lei, K., Xu, M., Shao, B., Wang, Y., Kong, Y. (2018). Ordered Mesoporous Silicas and Their Catalytic Applications in the Oxidation of Aromatic Compounds.

https://doi.org/10.3390/catal8020080

[18] Yang, H., Fang, J., Liu, L., Du, H. (2024). Research progress on photocatalytic degradation performance of CuS and its composite materials. *Materials Today Communications,* 40(May), 109988. DOI: 10.1016/j.mtcomm.2024.109988

[19] Porcu, S., Secci, F., Ricci, P.C. (2022). Advances in Hybrid Composites for Photocatalytic Applications : A Review. *Molecules,* 27, 6828. DOI: 10.3390/ molecules27206828

[20] Gao, S., Li, W., Dai, J., Wang, Q., Suo, Z. (2021). Effect of transition metals doping on electronic structure and optical properties of ß-Ga 2 O 3 Effect of transition metals doping on electronic structure and optical properties of ß - Ga 2 O 3. *Materials Research Express*, 8, 025904. DOI: 10.1088/2053-1591/abde10

[21] Patnaik, S., Sahoo, D.P., Parida, K. (2021). Recent advances in anion doped g-C 3 N 4 photocatalysts : A review. *Carbon*, 172, 682–711. DOI: 10.1016/j.carbon.2020.10.073.

[22] Characteristics, O. morphological , optical and magnetic The impact of nickel doping on the structural , morphological , optical and magnetic characteristics of zinc oxide nanorods. https://doi.org/10.1088/1742-6596/2974/1/012018

[23] Wang, Z., Wang, Z., Wang, J., Shi, H., Wang, C., Fan, Y., Bai, Z., Zhu, C. (2023). ScienceDirect Ni , Zn Co-doping ZIF-67-derived electrocatalyst based on CNT film for efficient overall water splitting. *International Journal of Hydrogen Energy*, 48(75), 29189–29197. DOI: 10.1016/j.ijhydene.2023.04.082.

[24] Chang, W., Jhan, D., Lu, J., Chen, S., Huang, Y., Chang, Y., Lu, M. (2025). Synergistic enhancement of photocatalytic hydrogen evolution via Ni doping and Mo_2C co-catalysis in $ZnIn_2S_4$. *Journal of Alloys and Compounds*, 1039(June), 183242. DOI: 10.1016/j.jallcom.2025.183242.

[25] Guo, B., Liu, L., Li, A., Li, X., Chang, Y., Jiao, Z., Han, M. (2024). Insights into the effect of Ni doping on In 2 S 3 for enhanced activity and selectivity of photocatalytic CO 2 reduction. 995(May) DOI: 10.1016/j.jallcom.2024.174741.

[26] Ranjan, N., Prakash, S., Sahu, D. (2026). Nickel ion doping induced enhancement in photocatalytic degradation efficiency of tin oxide nanoparticles towards mineralization of Reactive Blue 19 textile dye. *Next Materials*, 10(October 2025), 101362. DOI: 10.1016/j.nxmate.2025.101362.

[27] Li, Z., Zhang, L., Wang, L., Yu, W., Zhang, S., Li, X. (2023). Engineering the electronic structure of two-dimensional MoS 2 by Ni dopants for pollutant degradation. *Separation and Purification Technology*, 314(January), 123637. DOI: 10.1016/j.seppur.2023.123637.

[28] Morante, N., Monzillo, K., Padua, A., Muscatello, A., Sannino, D., Esposito, S., Vaiano, V. (2025). Engineered NiO / TiO 2 and CuO / NiO / TiO 2 heterojunctions for sustainable direct photocatalytic epoxidation of propylene using molecular oxygen. *Discover Nano*, 20, 104. DOI: 10.1186/s11671-025-04296-6.

[29] Belloni, C., Korving, L., Witkamp, G.J., Brück, E., Dugulan, A.I. (2024). Colloids and Surfaces A : Physicochemical and Engineering Aspects Zn induced surface modification of stable goethite nanoparticles for improved regenerative phosphate adsorption. *Colloids and Surfaces A: Physicochemical and Engineering Aspects*, 687(January), 133476. DOI: 10.1016/j.colsurfa.2024.133476.

[30] Alhamdu, I., Chidera, E., Mustapha, S., Saka, A., Oladejo, J. (2026). Adsorption kinetics , isotherm , and thermodynamics studies of phytochemical-assisted synthesized ZnO nanoparticles for the removal of selected heavy metals from abattoir wastewater. *Desalination and Water Treatment*, 325(December 2025), 101628. DOI: 10.1016/j.dwt.2025.101628.

[31] Liu, C., Zhu, Y., Di, S., He, J., Niu, P., Kelarakis, A., Krysmann, M., Wang, S., Li, L. (2024). coating for ultra - stable Zn metal anodes. https://doi.org/10.1002/elt2.29

[32] Dadi, D.G., Shura, M.W., Gochole, F. (2025). OPEN DFT analysis of structural , electronic and optical properties of Ni and Zn doped CoS counter electrode for dye sensitized solar cells. *Scientific Reports*, 15, 35486. DOI: 10.1038/s41598-025-19663-7 1

[33] Maria, L., Anna, S., Aravind, A., Ma, Y., Anil, S. (2023). Effect of Ni doping on the adsorption and visible light photocatalytic activity of ZnO hexagonal nanorods. *Inorganic Chemistry Communications*, 147(May 2022), 110208. DOI: 10.1016/j.inoche.2022.110208.

[34] Khan, S., Sadiq, M., Muhammad, N., Noor, A., Qayyum, S. (2026). NiCd / ZnO nanocomposites : novel materials for photocatalytic degradation of Allura Red dye. *Scientific Reports,* 16, 5204. DOI: 10.1038/s41598-026-36010-6 1.

[35] Rao, S., Shilpa, M.P., Shetty, S.J., Bhat, S.S., Gummagol, N.B., Surabhi, S., Gurumurthy, S.C. (2025). Zn - doped - TiO 2 nanoparticles : enhanced catalytic and nonlinear optical properties. *Journal of Materials Science: Materials in Electronics*, 36(19), 1–13. DOI: 10.1007/s10854-025-15182-3.

[36] Harsono, H., Nurhuda, M., Utami, T.S., Dardiri, A.A., Engge, Y., Maulana, F. (2023). EFFECT OF ADDITIONAL Ni METAL DOPANTS ON OPTICAL ABSORPTION PROPERTIES AND CRYSTAL STRUCTURE OF ZnO PHOTOCATALYST MATERIALS. *Jurnal Neutrino:Jurnal Fisika dan Aplikasinya,* 15(2), 52–61. DOI: 10.18860/neu.v15i2.17514.

[37] Li, Z., Yao, Y., Gao, X., Bai, H., Meng, X. (2021). Interfacial charge transfer

and enhanced photocatalytic mechanisms for Pt nanoparticles loaded onto sulfur-doped g-C 3 N 4 in H 2 evolution. *Materials Today Energy*, 22, 100881. DOI: 10.1016/j.mtener.2021.100881.

[38] Vento-lujano, E., Gonz, L.A. (2021). Applied Surface Science Defect-induced modification of band structure by the insertion of Ce 3 + and Ce 4 + in SrTiO 3 : A high-performance sunlight-driven photocatalyst. 569(June) DOI: 10.1016/j.apsusc.2021.151044.

[39] Zhao, Y., Cui, H., Xu, J., Shi, J., Yan, R., Yan, N. (2025). Synthesis of biomimetic N-doped porous carbons from gelatin using salt template coupled with chemical activation strategy for CO 2 capture. *Chemical Engineering Journal*, 505(January), 159241. DOI: 10.1016/j.cej.2025.159241.

[40] Rahmani, M., Pourmadadi, M., Abdouss, M., Rahdar, A. (2024). Industrial Crops & Products Gelatin / polyethylene glycol / g-C 3 N 4 hydrogel with olive oil as a sustainable and biocompatible nanovehicle for targeted delivery of 5-fluorouracil. *Industrial Crops & Products*, 208(December 2023), 117912. DOI: 10.1016/j.indcrop.2023.117912.

[41] Ulfa, M., Rohmah, I.S. (2025). Thermal-induced structural evolution of mesoporous oxides Fe – Co – Ni for enhanced visible-light dye degradation. *Next Materials*, 9(August), 101024. DOI: 10.1016/j.nxmate.2025.101024.

[42] Hasan, R., Muhammadi, F.M., Solihat, I., Listianti, E., Putri, Y.R., Alfiani, P. (2025). ARTICLE ORIGINAL Nano-silica Derived from Coal Fly Ash : A Sustainable Iron (III) Ion Adsorbent. 10(3), 331–338. DOI: 10.22090/jwent.2025.03.008.

[43] Ulfa, M., Aziza, H., Amalia, N. (2025). Results in Engineering In-situ sulfonated mesoporous silica as ZnO nanomaterial support for enhanced dyes photodegradation. *Results in Engineering*, 26(October 2024), 104381. DOI: 10.1016/j.rineng.2025.104381.

[44] Jabkhiro, H., Naitana, M.L., Marconi, E., Bertel, F., Iucci, G., Carlomagno, I., Battocchio, C., Meneghini, C., Tortora, L. (2025). One-Pot Synthesis of Zinc-Doped Mesoporous Silica. *Crystals*, 15, 100. DOI: 10.3390/cryst15020100.

[45] Zhao, Q., Hu, W., Li, S., Gu, Z., Zhang, Y., Yao, Y., Zhang, Y. (2023). Microporous and Mesoporous Materials Incorporation of metal organic framework into mesoporous silica nanoparticles with high contents. *Microporous and Mesoporous Materials*, 360(June), 112707. DOI: 10.1016/j.micromeso.2023.112707.

[46] Evdokimenko, N.D., Kapustin, G.I., Tkachenko, O.P., Kalmykov, K.B., Kustov, A.L. (2022). Zn Doping Effect on the Performance of Fe-Based Catalysts for the Hydrogenation of CO 2 to Light Hydrocarbons. *Molecules*, 27, 1065. DOI: 10.3390/ molecules27031065

[47] Guo, B., Liu, L., Li, A., Li, X., Chang, Y., Jiao, Z., Han, M. (2024). Insights into the effect of Ni doping on In 2 S 3 for enhanced activity and selectivity of photocatalytic CO 2 reduction. 995(April) DOI: 10.1016/j.jallcom.2024.174741.

[48] Mostafa, M., Khalifa, A., Hemeda, O.M., El, M.I.A., Sorory, H.A.-, Shalaby, R.M., Abdelhakim, N.A. (2025). A Comparative study of the influence of Zn ions as a growth catalyst on the physical and mechanical properties of MnFe 2 O 4. *Journal of Crystal Growth*, 653(December 2024), 128073. DOI: 10.1016/j.jcrysgro.2025.128073.

[49] Ahmed, W., Iqbal, J. (2021). Effect of Ni doping on structural , optical and magnetic characteristics of ZrO 2 nanoparticles with efficient visible light driven photocatalytic activity. *Ceramics International*, 47(17), 24895–24905. DOI: 10.1016/j.ceramint.2021.05.216.

[50] Ashokkumar, M., Muthukumaran, S. (2014). Microstructure , optical and FTIR studies of Ni , Cu co-doped ZnO nanoparticles by co-precipitation method. *Optical Materials*, 37, 671–678. DOI: 10.1016/j.optmat.2014.08.012.

[51] Tsai, J., Lee, T., Chiang, H. (2023). Nitrogen Adsorption and Characteristics of Iron , Cobalt , and Nickel Oxides Impregnated on SBA-15 Mesoporous Silica. *Nanomaterials*, 13, 1015. DOI: 10.3390/ nano13061015.

[52] Zhuang, J., Lu, B., Gu, F., Zhong, Z., Su, F. (2018). Ordered mesoporous Cu – Ca – Zr : A superior catalyst for direct synthesis of methyl formate from syngas. *Carbon Resources Conversion*, 1(2), 174–182. DOI: 10.1016/j.crcon.2018.05.005.

[53] Zienkiewicz-strzalka, M., Blachnio, M., Derylo-marczewska, A., Winter, S. (2024). Mesoporous Carbons and Highly Cross-Linking Polymers for Removal of Cationic Dyes from Aqueous Solutions — Studies on Adsorption Equilibrium and Kinetics. *Materials,* 17, 1374. DOI: 10.3390/ma17061374.

[54] Shen, J., Wu, C., Song, J., Yu, J., Li, Y. (2023). Adsorption and capillary condensation transitions on nanostructures : Mechanisms of atomic evolution and meniscus growth. *International Communications in Heat and Mass Transfer*, 148, 107064. DOI: 10.1016/j.icheatmasstransfer.2023.107064.

[55] Zhao, Y., Liu, X., Liu, Y., Chen, Y., Gao, S. (2022). ScienceDirect Favorable pore size distribution of biomass-derived N , S dual-doped carbon materials for advanced oxygen reduction reaction. *International Journal of Hydrogen Energy*, 47(26), 12964–12974. DOI: 10.1016/j.ijhydene.2022.02.064.

[56] Kumar, M., Ramulu, B., Yu, J.S. (2023). Nanoarchitectonic Ni-doped edge dislocation defect-rich MoS 2 boosting catalytic activity in electrochemical hydrogen production. *Journal of Cleaner Production*, 414(February), 137589. DOI: 10.1016/j.jclepro.2023.137589.

[57] Ungureanu, A., Dragoi, B., Chirieac, A., Ciotonea, C., Duprez, D., Mamede, A.S., Dumitriu, E. (2013). Composition-Dependent Morphostructural Properties of Ni − Cu Oxide Nanoparticles Con fi ned within the Channels of Ordered Mesoporous SBA-15 Silica. *Applied Maters & Interfaces*, 5, 3010−3025. DOI: 10.1021/am302733m

[58] Song, T., Du, X., Xia, T., Liu, Y., Zhu, J., Zhang, X. (2026). Effect of Fe / Ni Microalloying on Interface Regulation of SiC / Al Composites : Molecular Dynamics Simulation and Experiments. *Materials*, 19, 283. DOI: 10.3390/ma19020283.

[59] Ranjan, N., Prakash, S., Sahu, D. (2026). Nickel ion doping induced enhancement in photocatalytic degradation efficiency of tin oxide nanoparticles towards mineralization of Reactive Blue 19 textile dye. *Next Materials,* 10, 101362. DOI: 10.1016/j.nxmate.2025.101362

[60] Shi, Y., Chu, W., Zhang, L., Wang, B., Saidi, W.A., Zhao, J., Prezhdo, O. V (2025). Band Gap Narrowing in Lead-Halide Perovskites by Dynamic Defect Self-Doping for Enhanced Light Absorption and Energy Upconversion. https://doi.org/10.1021/acs.chemmater.4c02530

[61] Sadiq, M. (2022). Applied Surface Science Advances Ni 2 + grafted Ag 3 PO 4 : Enhanced photocatalytic performance under visible light. 11(June) DOI: 10.1016/j.apsadv.2022.100288.

[62] Kamarulzaman, N., Diyana, N., Aziz, A., Firdaus, M., Fadilah, N., Hanum, R., Subban, Y., Badar, N. (2019). Journal of Solid State Chemistry Anomalies in wide band gap SnO 2 nanostructures. 277(May), 271–280. DOI: 10.1016/j.jssc.2019.05.035.

[63] Zerjav, G., Zava, J. (2022). Journal of Environmental Chemical Engineering The influence of synthesis conditions on the visible-light triggered photocatalytic activity of g-C 3 N 4 / TiO 2 composites used in AOPs skari ˇ. 10(April) DOI: 10.1016/j.jece.2022.107656.

[64] Ishikawa, T., Matsuda, M., Inagaki, S., Fukushimab, T., Kondo, S. (1985). Surface silanol groups of mesoporous silica FSM-16. Faraday, 92. DOI: 10.1039/FT9969201985.

[65] Ai, L., Liu, Z., Zhang, X., Wang, L., Jia, D., Guo, N., Zha, M., Tan, C. (2025). Journal of Colloid And Interface Science Engineering cycling of Cu 2 + / Cu + pairs in Bi 2 WO 6 nanoflowers for boosting photocatalytic CO 2 reduction. *Journal of Colloid And Interface Science*, 692(December 2024), 137480. DOI: 10.1016/j.jcis.2025.137480.